8th GRACM International Congress on Computational Mechanics,
Volos, 12 July - 15 July 2015

A MULTI-CHANNEL MATHEMATICAL MODEL FOR PARTIALLY FAILED DIESEL PARTICULATE FILTERS

Onoufrios A. Haralampous and Dimitrios Mastellos

Department of Mechanical Engineering, Technological Educational Institute of Thessaly
Larissa, GR-41110, Greece
e-mail: onoufrios@teilar.gr; web page: http://www.heatlab.teilar.gr

Keywords: mathematical modeling, diesel particulate filters, partial failure, filtration efficiency, loading.

Abstract:

One of the latest developments in automotive emissions control is the adoption of new stringent On-Board Diagnosis (OBD) threshold limits for particulate mass. As a result, novel soot sensors are actively under development and extensive failure studies are underway aiming at the development reliable modern exhaust systems. To this end, the current work presents a transient multi-channel 1-d mathematical model for partially failed filters, combining conventional wall-flow filter modeling and recent developments in semi-open channel modeling. The latter is used to approximate the damaged region with channels missing rear plugs. Thus, the local flow rate, filtration efficiency and deposit loading are calculated as a function of time, for both the intact and failed region. The proposed model is first validated against steady-state CFD simulations using the porous medium approach for the monolith volume and then utilized to estimate the effect of failure level on backpressure and mass filtration efficiency of the filter. The overall results provide useful information about the expected performance of filters with various failure levels for several loading durations. Interestingly the deposit loading is shown to enlarge the negative effect of the damage on filtration efficiency, while the related pressure drop increase during loading is very modest in damaged filters compared to intact.

1 INTRODUCTION

The introduction of automotive emissions control in the early 1970s and the ongoing reduction of legislation limits all over the world have driven research in all areas of engine exhaust after-treatment. One of the latest developments is the adoption of new stringent On-Board Diagnosis (OBD) threshold limits for automotive emissions in several countries[1, 2]. In Europe the EURO 6 OBD threshold limit (OTL) for Particulate Mass (PM) has been defined at 12 mg/km (~ 2.5 the emission limit) with implementation dates starting in 2017. Likewise, heavy duty vehicles must comply to an OTL of 25 mg/kWh until 2016. As a result, Euro 6/VI applications should also identify partial Diesel Particulate Filter (DPF) failures and not only total failure as required by Euro 5/V[3]. Additionally particle number (PN) OTLs are also under discussion for diesel and GDI vehicles.

A filter failure is usually related with the harsh conditions of a regeneration event. Fig. 1a shows a cordierite filter with partially melted channels at the rear end due to temperatures above $1200^{\circ}C$. This situation can easily occur in cordierite filters, when the regeneration is initiated with excessive soot loading or the procedure is not properly controlled. Silicon carbide filters on the other hand are more resilient to temperature but prone to increased thermal stresses. Fig. 1b shows cracks developed at the rear end due to steep temperature gradients during a regeneration procedure. In both cases some of the inlet channels start to leak unfiltered exhaust gas directly to the environment, which is evident by the blackening of these channels. A partially failed filter is commonly studied experimentally by manually removing a fraction of the rear plugs, as shown in Fig. 1c. This way, it has been experimentally established that backpressure monitoring is not sufficient for on-board diagnosis of partially failed DPFs[4, 5]. Advanced diagnostic measures are necessary in the exhaust system to monitor the DPF filtration efficiency and tailpipe PM emissions [6]. As a result, novel soot sensors have recently been developed for filter diagnosis[7, 8, 6].

In this frame, modeling tools can facilitate the interpretation of the experimental measurements and provide further

insight into the behavior of a partially failed filter, supporting the development of efficient OBD systems. This paper presents a mathematical model able to predict filtration efficiency and pressure drop performance of partially failed filters. Furthermore the time-varying non-uniform accumulation of soot mass in the channels is calculated in order to predict the transient filter behavior throughout the operating cycle.

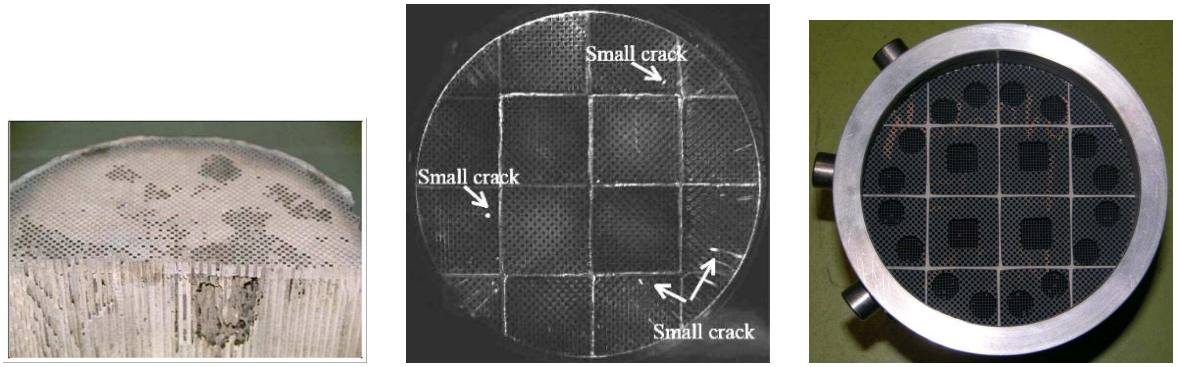

(a) Melted cordierite filter[9] (b) Cracked SiC filter[10] (c) SiC filter with manually removed rear plugs[11]

Figure 1: Clean filter filtration efficiency as a function of failure level.

2 MATHEMATICAL MODEL

The fundamentals of wall-flow filter modeling were established in the early 80s[12]. Since then DPF models have been further refined and thoroughly validated [13, 14]. In order to extend this model to partially failed filters, recent developments in partial wall-flow filters modeling[15, 16] are used. As a result, the damaged region is numerically approximated with channels missing rear plugs using modified boundary conditions.

A multi-channel approach is applied to account for the intact and failed zones separately. ϕ_j is defined as the fraction of frontal area (or channels) included in each zone, defined as:

$$\phi_j = \frac{A_j}{A} = \frac{N_j}{N}, \quad j = I, F \tag{1}$$

Subscripts I and F are used for the intact and failed zone respectively, while the absence of subscript denotes reference to the complete filter. For convenience ϕ_F is referred as failure level.

2.1 Continuity equation and momentum balance

Assuming uniform radial behavior of all channels, the control volume can be reduced to a pair of inlet and outlet channels for each zone, as shown in table 1. A common system of equations is used for the calculation of the flow field in both zones. The continuity equation is expressed as:

$$\frac{\partial}{\partial z}\left(\rho u_i D^2\right) = (-1)^i \, 4D\rho u_w, \quad i = 1, 2 \tag{2}$$

where i is the channel index, 1 denoting inlet channel and 2 outlet.

Assuming a sufficiently small deposit layer gradient, the momentum balance is expressed as:

$$\frac{\partial p_i}{\partial z} + \frac{\partial}{\partial z}\left(\rho u_i^2\right) = -\frac{\alpha_1 \mu u_i}{D^2}, \quad i = 1, 2 \tag{3}$$

while a Darcy pressure drop term is used for the wall flow between the channels:

$$p_1 - p_2 = \frac{\mu u_w w}{k} \tag{4}$$

The resistance term w/k includes all the layers in series, usually substrate and cake:

$$\frac{w}{k} = \frac{w_c}{k_c} + \frac{w_s}{k_s} \, . \tag{5}$$

The contraction and expansion pressure losses are also taken into account with the following expressions [17]:

$$\Delta p_{contraction} = \left[1.1 - 0.4\frac{{d_{h0}}^2}{\left(d_c + w_w\right)^2}\right]\frac{\rho {u_{p0}}^2}{2} \tag{6}$$

$$\Delta p_{expansion} = \left[1 - \frac{{d_{hL}}^2}{\left(d_c + w_w\right)^2}\right]^2\frac{\rho {u_{pL}}^2}{2} \tag{7}$$

Constant gas density is assumed throughout the monolith based on the small pressure variations expected in real-life applications.

Channel	Schematic	Boundary conditions
Intact	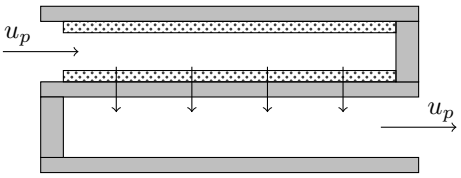	$u_1(0) = u_p$ $u_2(0) = 0$ $u_1(L) = 0$ $p_2(L) = p_{out}$
Failed	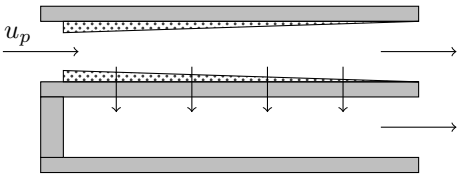	$u_1(0) = u_p$ $u_2(0) = 0$ $p_1(L) = p_{out}$ $p_2(L) = p_{out}$

Table 1: Boundary conditions

In order to solve the system of differential eqs (2) to (7), the boundary conditions at the inlet and outlet face are defined according to table 1. The flow rate for each zone and the outlet pressure are assumed known. Of note, the failed case boundary conditions differ in the rear, where the exit velocity of channel 1 is unknown and has been replaced by a pressure definition.

2.2 Particle mass balances

Diesel particle distributions typically cover ranges starting from a few nm and extending up to several hundreds, with a maximum around $100nm$. At these sizes, the bulk of the particles are expected to follow the gas streamlines, a common assumption employed in conventional wall-flow modeling. At quasi-steady state conditions the particle balance inside the channels can be expressed with the following differential equations:

$$\begin{aligned}\frac{\partial}{\partial z}\left(u_m {d_h}^2 C_1\right) &= -4 d_h \rho u_w C_1 \\ \frac{\partial}{\partial z}\left(u_m {d_h}^2 C_2\right) &= 4 d_h \rho u_w C_w\end{aligned} \tag{8}$$

The concentration of the flow that changes channel C_w is further reduced due to the surface and deep-bed filtration at the deposit layer and wall:

$$C_w = \left(1 - \eta_{f,W}\right) C_1 \tag{9}$$

A very common method to account for the aerosol distribution is to use multiple particle classes corresponding to different particle diameters[18]. In the general case, the above differential equations constitute a system that has to be solved independently for each particle class.

The evolution of deposit loading θ_1 at a specific axial location is a function of local wall velocity, wall filtration efficiency and particle concentration:

$$\frac{\partial \theta_1}{\partial t} = s \sum_{classes} (u_w C_1 \eta_{f,W}) \tag{10}$$

$$\tag{11}$$

Finally the accumulation rate is summed for all particle classes.

3 NUMERICAL METHODS

The presented multi-channel 1-dimensional transient mathematical model can be solved with basic finite volume techniques[19]. A constant discretization step of $2mm$ is used for the axial distance. The steady boundary conditions allows the usage of rather large time step, which was set at $60s$ The initial state was assumed clean and the loading simulations were terminated at $3h$. For each time step, an iterative flow field calculation was followed by a direct calculation of particle mass balances. The algorithm was implemented as a code in Fortran 2003[20] and was initially tested with analytical solutions.

3.1 Flow field

The flow field calculation takes place in two discrete steps representing the channel scale and filter scale. Equivalent electrical circuits are used in both steps, resulting in very short calculation times.

At the channel scale, the equivalent circuit includes two parallel channels, with resistances placed horizontally for channel flow and vertically for wall-flow. Eqn (3) is used to determine the axial resistances, using initial flow estimates denoted with an asterisk to linearize the momentum term. For a discrete channel length, the channel resistance is expressed as:

$$R_i = \frac{p_i(z) - p_i(z+\Delta z)}{\dot{m}_i} = \frac{\alpha_1 \mu \Delta z + 2\left[\dot{m}_i{}^*(z+\Delta z) - \dot{m}_i{}^*(z)\right]}{\rho {d_h}^4 \phi_j N} \, , i = 1,2 \tag{12}$$

Infinite resistance values are used at plug locations while eqn(4) is discretized to extract the traverse resistance as:

$$R_w = \frac{p_2 - p_1}{\dot{m}_w} = \frac{\mu \frac{w}{k}}{\rho \phi_j N 4 d_h \Delta z} \tag{13}$$

In both expressions the channel fraction ϕ of each zone is taken into account. A total resistance can then be calculated from the complex circuit, yielding the total pressure drop and the flow field in a pair of channels. In case of significant divergence from the initial estimate, the procedure is repeated. Typically 2 to 6 iterations are necessary for a relative accuracy of 10^{-6}, using the flow field of the previous time step as an initial guess.

The resistance approach can also be employed to solve the flow distribution at the inlet face[21]. The total pressure drop calculated for each zone at the previous step is used to estimate the two resistances:

$$R_j = \frac{{\Delta p_j}^*}{\dot{m}_j^*} \tag{14}$$

These resistances are arranged in parallel, hence the mass flow distribution is given as:

$$\dot{m}_I = \frac{R_F}{R_F + R_I} \dot{m} \tag{15}$$

$$\dot{m}_F = \frac{R_I}{R_F + R_I} \dot{m} \tag{16}$$

Since the mass flow rates are initially unknown, flow rate estimates $\dot{m}_j^*$ are used initially to calculate a temporary pressure drop ${\Delta p_j}^*$. This leads to an iterative calculation of the flow rates, which typically requires 2 to 4 iterations to converge with a tolerance limit of 10^{-5}.

3.2 Particle mass balances

As already mentioned, the aerosol distribution can be approximated with multiple particle classes. The inlet diameter range is divided into 32 intervals, which are equidistant in logarithmic scale. All the properties are calculated at the central diameter of the interval. The measured number value can then be converted to mass concentration for each class, using the effective particle density.

The quasi-steady state particle balance in the channel (eqn (9)) is a parabolic differential equation, which can be numerically integrated until the end of the channel for each class. A staggered grid is used with concentrations calculated at cell faces, while deposit loading and source terms are calculated at cell centers. Locally integrated expressions are applied sequentially for all calculation cells, yielding the concentration C along the inlet and outlet channel. Next the deposit balance (eqn (11)) is integrated in time to yield the evolution of deposit mass. There are no direct interactions from neighboring cells and the new deposit values can be calculated explicitly with a sufficiently small time step.

4 SAMPLE RESULTS

A series of loading simulations are presented in this section to demonstrate the capabilities of the model. The design parameters and boundary conditions of the filter under investigation are given in Ref. [15]. The loading duration has been set to $3h$, while the PM emission rate is assumed $5g/h$. In order to simplify the problem, complete filtration has been assumed at the wall ($\eta_f = 100\%$) for all particles. This assumption is generally very close to reality with some exceptions related to completely clean state [22, 23]. Furthermore a deposit density of $80kg/m^3$ has been used for both zones.

4.1 Clean state

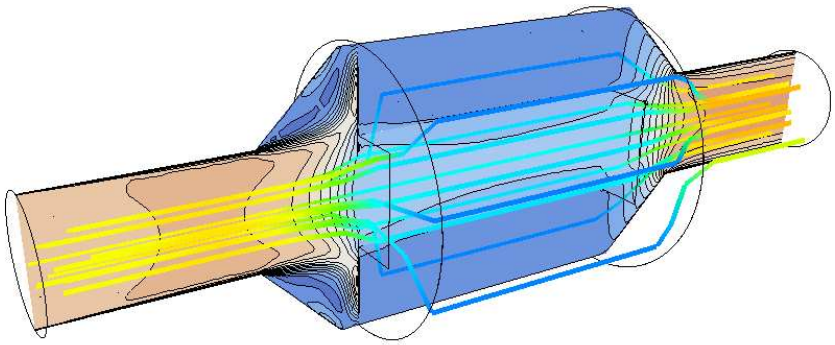

Figure 2: Streamlines and velocities in a filter with 20% failure level.

The performance of a clean filter with partial failure is presented first to facilitate better understanding. Following our previous work[15], a commercial CFD package[24] was used to calculate the steady-state flow field of a clean filter. An inlet and outlet cone were included in the control volume, while the filter was modeled as a porous medium. Analytical expression were used to determine the porous flow resistance in the intact and compromised zone. This set of simulations has been extended in this study with additional failure levels. A typical result is shown in Fig. 2 for a filter with a square damaged zone at the center, covering 20% of the channels. As expected, the flow concentrates at the center. Given that the average steady-state calculation time using CFD was about $1h$, the CFD results are used here only as a validation for the multi-channel model (MCM). The MCM can then be used for transient simulations, which typically last only a few seconds.

The flow fraction entering the intact zone is shown as a function of failure level in Fig. 3. It decreases at higher

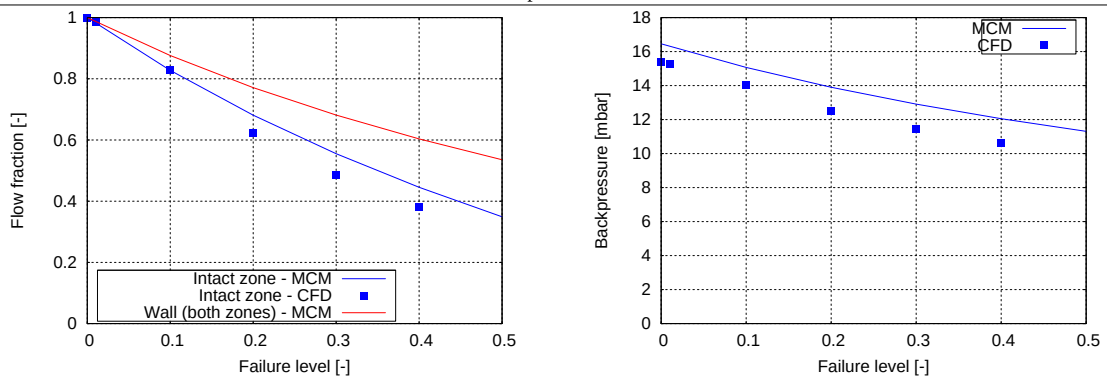

(a) Flow distribution as a function of failure level.

(b) Backpressure as a function of failure level.

Figure 3: Flow performance at clean state as a function of failure level.

failure levels, as flow is increasingly diverged through the damaged channels due to their comparatively lower resistance. The MCM agrees well with the CFD results and a small divergence could be attributed to the effect of the inlet and outlet cones, not accounted for in the MCM. All of the flow passing through the intact region is forced through the wall, thus achieving 100% filtration efficiency. Additionally about 30% of the flow entering the damaged channels passes through the wall, thus increasing the total wall flow fraction. Fig. 3b shows the calculated pressure for both approaches as a function of failure level. As expected, lower backpressure appears at higher failure levels. Again the two models exhibit consistent trends albeit with a small deviation that extends in the complete range of failure levels. This difference is attributed to the contraction/expansion losses not included in the CFD and the usage of analytical expressions for the porous resistances.

4.2 Loading

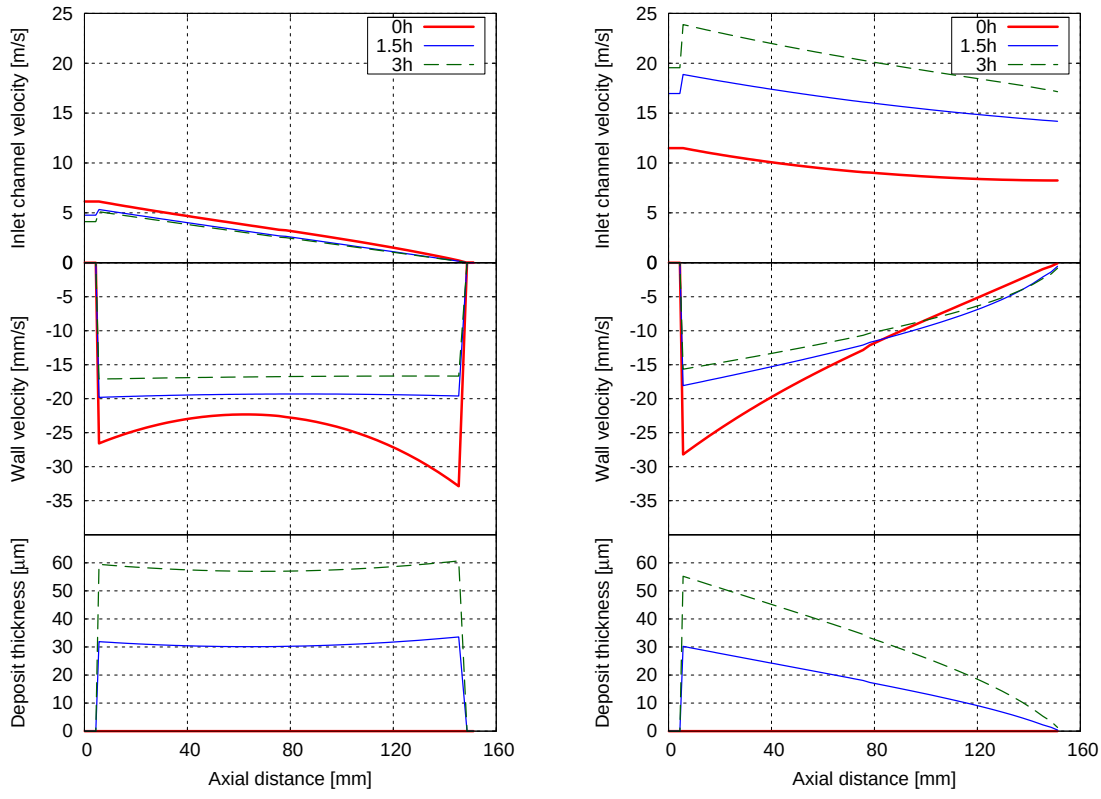

(a) Intact zone

(b) Failed zone

Figure 4: Velocity and deposit thickness profiles in a filter with 20% failure level.

During the loading phase deposit accumulates in both zones affecting the flow field. Fig. 4 depicts the velocity and deposit thickness profiles at 3 time points for both zones. The upper section presents the inlet channel velocity. In the intact inlet channel (Fig. 4a), the entrance velocity is about $5m/s$ and reduces to zero at the end of the channel, while the velocity level decreases slightly as time passes. In the damaged channel (Fig. 4b), flow enters initially with an axial velocity above $10m/s$ and exits the channel with about $8m/s$ as a result of the missing plug. The axial velocities increase considerably with time, while maintaining the same qualitative profile.

The inlet channel velocities are consistent with the wall velocities shown in the middle section of the same graph. The wall velocity profile is initially curved in the intact channel but becomes uniform at $t = 1.5h$ and $t = 3h$, while slightly reducing. Of note, the wall velocity value close to the entrance is almost the same in both channels for all time points. However the wall velocity profiles in the failed zone approach linear behavior reaching zero close to the filter exit.

With the exception of the clean state, the deposit thickness profile (lower section of the graph) is a reflection of the wall velocity profile. This is expected, as the local deposit loading increases proportionally to the local wall velocity. Furthermore the deposit layer is an extra resistance for the wall velocity. As a result, wall velocities in both zones deteriorate with time at the expense of the direct axial flow in the damaged inlet channel (top section of right graph).

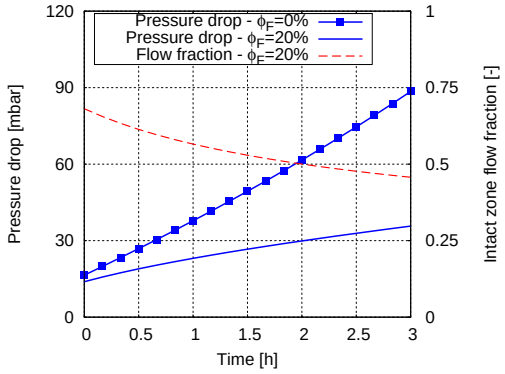

(a) Pressure drop and flow fraction as a function of time

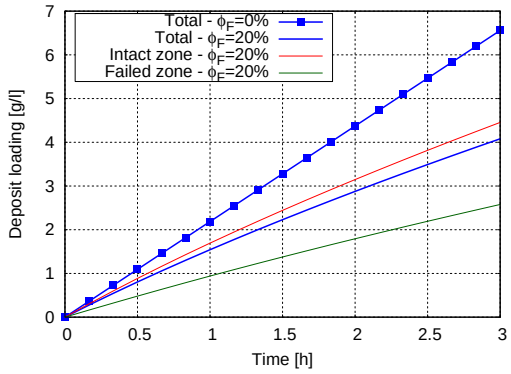

(b) Deposit loading as a function of time

Figure 5: Pressure drop, flow fraction and deposit loading of a filter with 20% failure level as a function of time.

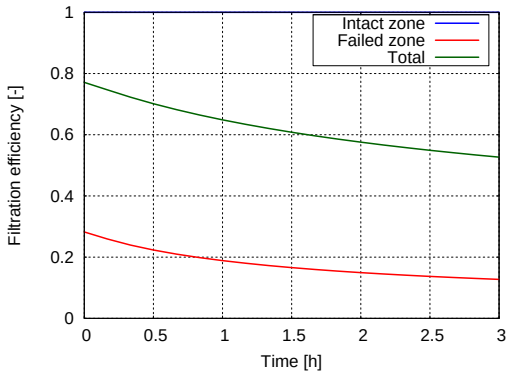

(a) Filtration efficiency as a function of time

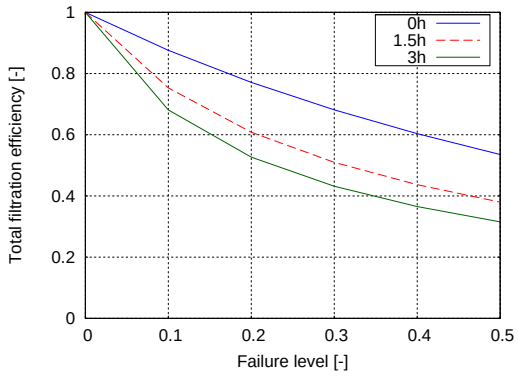

(b) Filtration efficiency as a function failure level

Figure 6: Filtration efficiency as a function of time and failure level.

The time-dependent redistribution of the flow is more clearly depicted in Fig. 5a. Due to the deposit buildup, the failed zone is gradually attracting more flow. For the same reason pressure drop increases, although very modestly compared to an intact filter. At the same time the deposit accumulates unevenly between the two zones (Fig. 5b), resulting in roughly double local loading in the intact zone. The total loading in the damaged filter is gradually diverging from the intact, which amounts to about $4g/l$ in the failed filter versus $6.5g/l$ expected in an intact filter after $3h$ of loading.

Fig. 6a shows the evolution of filtration efficiency. Taking into account the deposit buildup and increased velocities in the failed zone, the local filtration efficiency deteriorates very soon from 28% to 13%. The filtration efficiency of

the intact zone remains at 100%, however with decreasing contribution to the total efficiency due to the unfavorable flow redistribution. Finally Fig. 6b outlines the effects of failure level and loading duration. As discussed already, increased damage results in lower instantaneous filtration efficiency. This negative effect is enlarged considerably after a short period of loading ($1.5h$) and at moderate durations the filtration efficiency might even drop to half of the initial (e.g. $3h$ loading of a filter with 50% failure level). These results agree qualitatively with experimental measurements presented in the literature[4, 11].

5 CONCLUSIONS

A mathematical model for partially failed diesel particulate filters has been presented in this study. This model is characterized by a multi-channel approach to describe separately the intact and failed region. A solution method based on an equivalent electrical circuit has been proposed for the calculation of the flow field, while the finite volume approach is used to calculate the local particle concentrations and transient deposit loadings. The multi-channel model was initially validated with a few steady-state CFD simulations of clean filters and then employed in transient simulations requiring very short calculation times. This way, the transient simulations provided detailed performance information for a wide range of failure levels.

The transient results helped to clarify the filtration and flow redistribution mechanisms in the filter. Uniform wall velocity profiles occur in the intact region, while linear profiles arise in the failed region. In both cases the wall velocity magnitudes are gradually decreasing with time at the expense of the flow following a direct path to the ambient through the damaged channels. The variation of flow field inside the intact and damaged channels is also directly related to the profile of the deposit layer that forms during the loading phase.

The overall results provided useful information about the expected performance of filters with various failure levels at several time points of the loading phase. Interestingly the deposit loading is shown to enlarge the negative effect of the damage on filtration efficiency, while pressure drop increases very modestly in damaged filters compared to intact.

REFERENCES

[1] California Code of Regulations (2013), Title 12, Section 1968.2, OAL File No. 2013-0627-02S.

[2] Commission Regulation (EU) No 459/2012 of 29 May 2012, *Official Journal of the European Union* L 142/16.

[3] Steininger, N. (2010), ”On Board Diagnostics Legislation for Euro 6/VI Light and Heavy Duty Vehicles in Europe”, *SAE On-Board Diagnostics Symposium*, November 9-10, 2010, Amsterdam, Netherlands.

[4] Finch, S., Hnilicka, B. and Sindano, H. (2010), *EURO6 LightDuty Vehicle OBD Project: Evaluation and Assessment of Proposed EOBD Emission Thresholds* ACEA report Q51760, RD.10/320201.4

[5] Samaras, Z. (2010), ”On Board Diagnostics Legislation for Euro 6/VI Light and Heavy Duty Vehicles in Europe”, *On-Board Diagnostics Symposium*, Indianapolis, USA, August 24-26.

[6] Masoudi, M., and Sappok, A.G. (2014) ”Soot (PM) Sensors”, *Dieselnet Technology Guide*, http://www.dieselnet.com, rev. 2014.07 (assesed 5 March 2015).

[7] Ochs, T., Schittenhelm, H., Genssle A. and Kamp B. (2010), ”Particulate Matter Sensor for On Board Diagnostics (OBD) of Diesel Particulate Filters (DPF)”, *SAE paper* 2010-01-0307.

[8] Ntziachristos, L., Fragkiadoulakis, P., Samaras, Z., Janka, K. and Tikkanen, J. (2011), ”Exhaust Particle Sensor for OBD Application”, *SAE paper* 2011-01-0626.

[9] Majewski, W.A. (2015) ”Diesel Filter Systems”, *Dieselnet Technology Guide*, http://www.dieselnet.com, rev. 2015.03 (assesed 5 March 2015).

[10] Vogt, C.D., Shfer-Sindliger, A., Hashimoto, S., Hamanaka, T. and Matsubara, R. (2002), ”Dieselpartikelfilter mit optimierter Porosität fr beschichtete und unbeschichtete Dieselpartikelfiltersysteme”, *Aachener Kolloquium Fahrzeug- und Motortechnik*.

[11] Samaras Z., Geivanidis S., Vonk W., Anderson J., Sindano H., Hausberger S. and Perujo A. (2013), ”Testing of soot sensors for DPF failure monitoring”, *17th ETH conference on Combustion Generated Nanoparticles*, Zürich, Switcherland, 23-26 June.

[12] Bissett, E.J. (1984) ”Mathematical model of the thermal regeneration of a wall-flow monolith diesel particulate filter”, *Chemical Engineering Science* Vol. 39, Nos 7/8, pp. 1233-1244.

[13] Koltsakis, G., Haralampous, O., Depcik, C. and Ragone JC. (2013), ”Catalyzed diesel particulate filter modeling”, *Rev Chem Eng* 2013; 29(1): 1-65.

[14] Konstandopoulos, A.G., Kostoglou, M., Vlachos, N. et al. (2008), ”Advances in the Science and Technology of Diesel Particulate Filter Simulation”, *Advances in Chemical Engineering*, 33.

[15] Haralampous, O.A. and Kontzias, T. (2014), ”Approximate Pressure Drop and Filtration Efficiency Expressions for Semi-Open Wall-Flow Channels”, *Canadian Journal of Chemical Engineering*, Vol. 92, pp. 1517-1525.

[16] S. Basu, M. Henrichsen, P. Tandon, S. He, A Heibel (2013),”Filtration Efficiency and Pressure Drop Performance of Ceramic Partial Wall Flow Diesel Particulate Filters”, *SAE Int. J. Fuels Lubr.* 6(3), doi:10.4271/2013-01-9072.

[17] Haralampous, O.A., Kandylas, I.P., Koltsakis G.C. et al. (2004), ”Diesel particulate filter pressure drop Part 1: Modelling and experimental validation”, *Journal of Engine Research* 5, 2: 149-162, JER 02202.

[18] Hinds, WC (1999) *Aerosol technology: properties, behavior, and measurement of airborne particles*, New York, Wiley.

[19] Patankar, SV (1980), *Numerical Heat Transfer and Fluid Flow*, Taylor and Francis.

[20] Metcalf, M., Reid, J. and Cohen, M. (2011) *Modern Fortran explained*, Oxford University Press.

[21] Tsinoglou, D.N., Koltsakis, G., Missirlis, D.K. and Yakinthos, K.J. (2004), ”Modelling of flow distribution during catalytic converter light-off”, *International Journal of Vehicle Design*, Vol. 34(3), pp. 231-259.

[22] Bollerhoff, T., Markomanolakis, I. and Koltsakis, G. (2012), ”Filtration and regeneration modeling for particulate filters with inhomogeneous wall structure”, *Catalysis Today*, Vol. 188, pp. 2431.

[23] Zhong, D., He, S., Tandon, P., Moreno, M. and Boger, T. (2010), ” Measurement and Prediction of Filtration Efficiency Evolution of Soot Loaded Diesel Particulate Filters”, *SAE paper* 2012-01-0363.

[24] STAR-CCM+ 8.06 (2013), CD adapco, Melville.

Department of Mechanical Engineering
Technological Educational Institute of Thessaly
Larissa, GR-41110, Greece
email: onoufrios@teilar.gr